Model-based Analysis of Fixed-bed and Membrane Reactors of Various Scale

Jan P. Walter[1],*, Andreas Brune[1,2], Andreas Seidel-Morgenstern[1,3], and Christof Hamel[1,2]

Supporting Information
available online

A packed-bed membrane reactor in a distributor configuration is studied theoretically for the oxidative propane dehydrogenation and compared with a fixed-bed reactor. Based on detailed 2D models considering two different heat and mass transport models the reactor scale-up including various reactor-to-particle diameter ratios (D/d_P) is analyzed with respect to reactor performance, heat transfer and hot spot formation. Higher selectivities at lower hot spot temperatures occur in the packed-bed membrane reactor for the same reaction conditions.

1 Introduction

One major problem in chemical engineering is the occurrence of undesired side reactions, which reduce process efficiency [1, 2]. To avoid consecutive reactions, e.g., optimization is needed, considering the catalyst, the temperature, concentrations and the residence time [3–5]. To enhance selectivity and yield, process intensification in integrated reactors can be beneficial [6, 7]. Thereby, the chemical reaction is coupled with at least one additional unit operation in the same apparatus, according to the multifunctional reactor concept [8–11].

An example for multifunctional reactors is the packed-bed membrane reactor (PBMR), which combines in situ compound separation or dosing with chemical reaction. Applied to heterogeneously catalyzed gas phase reactions, a distributor regime can be used to lower the concentration of one reactant, thus, serial reactions of desired intermediates can be repressed and higher intermediate selectivities occur [12, 13]. In particular, in oxidative dehydrogenations (ODH), coupled with highly selective thermal dehydrogenations (TDH), a distributed dosing of oxygen is an interesting alternative to enhance the alkene selectivity by lowering the local oxygen concentration in comparison to a conventional fixed-bed reactor operation (FBR) [1, 14–16].

The ODH is an irreversible exothermic reaction [14]. Unfortunately, the heat of reaction leads to a hot spot formation. This problem increases dramatically during reactor scale-up. Reasons are the reduction of the surface-to-volume ratio, the flow maldistribution and the complex heat and mass transfer [17, 18].

In order to analyze and evaluate differences in reactor performance between the PBMR in distributor configuration and the conventional FBR, in this contribution detailed 2D-simulations were carried out for the ODH of propane to propene. If a radial flow is realized by a distributed dosing in a PBMR, the convective heat and mass transfer through the reactor wall and the porosity distribution have to be taken into account. For this, literature provides two established heat and mass transfer models of various complexity, the α_W model and the $\lambda(r)$ model [19–21]. The main difference between both models is the consideration of a constant porosity in the α_W model in contrast to a radial porosity profile in the $\lambda(r)$ model. Thus, differences in heat, mass and momentum transport result. The dependency between hot spot magnitude and localization on reactor scales is studied using both models.

[1]Jan P. Walter, Andreas Brune, Prof. Andreas Seidel-Morgenstern, Prof. Christof Hamel
jan.walter@ovgu.de
Otto von Guericke University Magdeburg, Institute of Process Engineering, Universitätsplatz 2, 39106 Magdeburg, Germany.

[2]Andreas Brune, Prof. Christof Hamel
Anhalt University of Applied Sciences, Process Engineering, Bernburger Straße 55, 06354 Köthen, Germany.

[3]Prof. Andreas Seidel-Morgenstern
Max Planck Institute for Dynamics of Complex Technical Systems, Sandtorstraße 1, 39106 Magdeburg, Germany.

2 Modelling

2.1 Balance Equations

For a detailed analysis of the temperature and concentration profiles in FBR and PBMR, a 2D reactor model is implemented in the commercial software tool COMSOL Mutliphysics® 5.5. The reactor model is based on the following assumptions: steady-state, pseudo-homogenous, ideal gas behavior, incompressible flow and no heat radiation.

2.1.1 Component Mass Balance

$$0 = -\frac{\partial(\varepsilon u_z c_i)}{\partial z} - \frac{1}{r}\frac{\partial(\varepsilon r u_r c_i)}{\partial r} + D_{i,z}^{eff}(r)\frac{\partial^2 c_i}{\partial z^2} + \frac{1}{r}\frac{\partial}{\partial r}\left[D_{i,r}^{eff}(r)r\frac{\partial c_i}{\partial r}\right] + (1-\varepsilon)\Phi\rho_{cat}\sum_{j=1}^{M}\nu_{i,j}r_j \tag{1}$$

$$\text{with} \quad \Phi = \frac{m_{cat}}{m_s} \tag{2}$$

$$\text{BC:} \quad c_i(z=0) = c_{i,ts}; \quad \frac{\partial c_i}{\partial z}(z=Z)=0; \quad \frac{\partial c_i}{\partial r}(r=0)=0 \tag{3}$$

$$\text{FBR:} \quad J_i = 0 \tag{4}$$

$$\text{PBMR:} \quad J_i = -D_{i,r}^{eff}\frac{\partial c_i}{\partial r}(r=R) \tag{5}$$

The molar flux through the membrane wall is calculated as follows:

$$J_i = \frac{\dot{V}_{ss}}{A_{mem}}c_{i,ss} \tag{6}$$

with the volumetric flow through the membrane $\dot{V}_{ss}$, the membrane surface area A_{mem} and the inlet concentration of component i distributed via membrane $c_{i,ss}$.

2.1.2 Heat Balance

$$0 = -c_{p_f}\frac{\partial(\varepsilon u_z \rho_f T)}{\partial z} - \frac{1}{r}c_{p_f}\frac{\partial(\varepsilon r u_r \rho_f T)}{\partial r} + \lambda_z^{eff}(r)\frac{\partial^2 T}{\partial z^2} + \frac{1}{r}\frac{\partial}{\partial r}\left[\lambda_r^{eff}(r)r\frac{\partial T}{\partial r}\right] + (1-\varepsilon)\Phi\rho_{cat}\sum_{j=1}^{M}(-\Delta H_R)_j r_j \tag{7}$$

$$\text{BC:} \quad T(z=0)=T_{in}; \quad \frac{\partial T}{\partial z}(z=Z)=0; \quad \frac{\partial T}{\partial r}(r=0)=0 \tag{8}$$

$$\alpha_W \text{ model } (\bar{\varepsilon}\neq f(r)): \quad -\lambda_r^{eff}\frac{\partial T}{\partial r}(r=R)=\alpha_W(T(r=R)-T_W) \tag{9}$$

$$\lambda(r) \text{ model } (\varepsilon = f(r)): \quad T(r=R)=T_W \tag{10}$$

The α_W model is based on radial constant dispersion coefficients for heat and mass transfer and a heat transfer coefficient, to describe the temperature rise in the wall-near region [20–23]. The more realistic $\lambda(r)$ model considers a radial dependency of the dispersion coefficients and heat transfer by conduction in the flow boundary layer [19–21].

2.1.3 Momentum Balance

To model the convective heat and mass transport dependency on the porosity distribution, the Navier-Stokes equations and the mass continuity equation are solved simultaniously in addition to the mass balances and heat balance as described in the Supporting Information 2.1.

2.2 Preliminary Investigations

2.2.1 Reactor Concepts and Reaction Network

In Fig. 1a the concepts of FBR and PBMR are illustrated. The reactor is divided in an inlet zone ①, a reaction/mem-
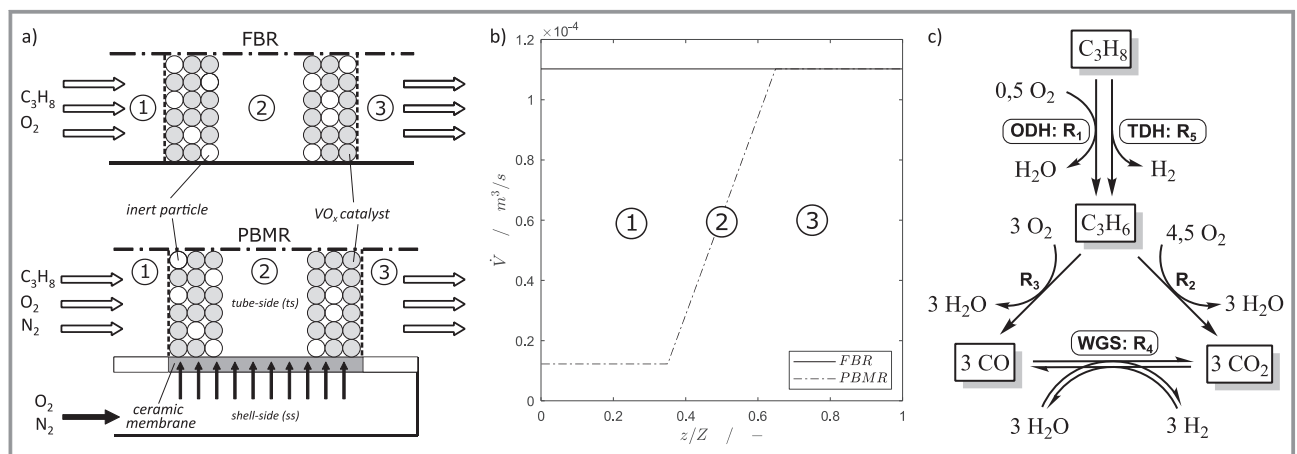
Figure 1. a) Schemes of studied reactor concepts FBR and PBMR, b) total volumetric flows of FBR and PBMR along axial reactor coordinate and c) reaction network of the ODH.

brane zone ② and an outlet zone ③. The comparability of both reactor concepts is given by the same volumetric flow ($\dot{V}$) at the outlet without reactions (Fig. 1b). Therefore, a splitting of the total volumetric flow in the PBMR case is necessary:

$$\dot{V}_{ts} = \frac{\dot{V}}{1 + \frac{1}{ts/ss}}; \quad \dot{V}_{ss} = \dot{V}_{ts} \frac{1}{ts/ss} \quad (11)$$

with the tube-to-shell-side ratio ts/ss, and the volumetric flow of the tube-side $\dot{V}_{ts}$.

The kinetic description for the ODH of propane is based on the derived reaction network, shown in Fig. 1c. Detailed information about the reaction kinetics can be found in Supporting Information 1.

### 2.2.2 Modelling of Heat and Mass Transfer

For an objective comparison and analysis of FBR and PBMR, taking into account scale-up, hot spot formation and cooling by distributed dosing, the 2D models (Eq. (1)–(10)) are solved applying the α_W model and the $\lambda(r)$ model. Since the more precise $\lambda(r)$ model, considering $\varepsilon = f(r)$, is in a better agreement with experimental data, it is used in the following for further investigations with respect to scale-up. Detailed information and discussions can be found in Supporting Information 2.2.

3 Simulation Studies

3.1 Influence of Reactor Scale-up

The surface-to-volume-ratio of cylindrical reactors decreases linearly with an increased tube diameter (4/D). This results in a greater distance between core and reactor wall, which leads to significant hot spot in packed catalyst beds during scale-up. To quantify this influence, various D/d_P ratios (6, 21, 40) of the FBR are studied with respect to hot-spot temperature and reactor performance. Two different cases are investigated: a constant weight hourly space velocity (WHSV = $m_{cat}/\dot{V}$) of $400\,\text{kg s m}^{-3}$ with an adjusted catalyst fraction Φ (Eq. (2)) (Supporting Information 3) and a constant catalyst fraction $\Phi = 1$ with an adjusted WHSV, as shown in Fig. 2 (calculations in Supporting Information 4). To assure a comparability between both cases, the same volumetric flow is used, so that the residence times are equal. The particle diameter is held constant at $d_P = 1\,\text{mm}$ [14].

As shown in Fig. 2, the reactor performance is enhanced due to an increased hot spot temperature during scale-up (266 K), supporting the endothermic TDH and catalyst deactivation by sintering, e.g. The maximum propene yield is reached at $D/d_P = 40$ and is about 45 %. The highest propene selectivities and yields occur independently of the reactor scale at very low oxygen concentrations ($x_{O2,in} = 0.25...1$ %), thus, the advantage of a PBMR in distributor
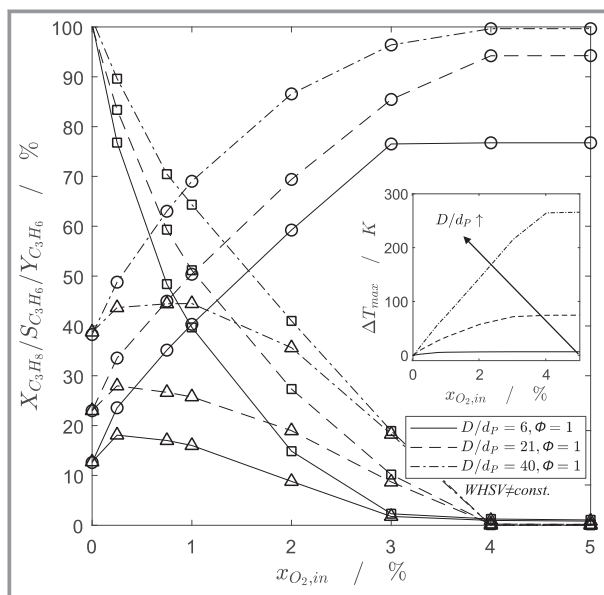
**Figure 2.** Conversion ○, selectivity □, yield △ and hot spot temperatures of various reactor scales of the FBR for different oxygen concentrations ($x_{C3H8,in} = 1$ %, $T_W = T_{in} = 600\,°\text{C}$, $d_P = 1\,\text{mm}$), $\lambda(r)$ model.

configuration is obvious. By applying distributed dosing, the membrane flow offers additionally the possibility to decrease the hot spot temperature by a convective cooling. Based on these finding, in the following chapter the impact of temperature by a radial dosing on hot spot formation and reactor performance is studied for various scales and compared with results of the FBR.

3.2 Influence of Constant Wall/Membrane Flow Temperature

The different dosing strategies are compared for a constant inlet and wall temperature ($T_W = T_{in} = 600\,°\text{C}$), a constant average reactor scale ($D/d_P = 21$) and different catalyst fractions and oxygen concentrations.

As shown in Fig. 3a and b, the oxygen dosing leads to an enhanced reactor performance of the PBMR in comparison to the FBR. In particular, the propene selectivity can be improved because of the lowered oxygen concentrations. Thus, undesired series reactions are depressed. However, due to higher local oxygen concentrations in the FBR, higher propane conversions occur. Since the propene yield of the PBMR is higher, it can be seen, that increased selectivities of the PBMR dominate higher conversions of the FBR. The yield can be enhanced up to 35 % by increasing the mass of catalyst, leading also to higher hot spot temperatures, especially in the conventional FBR (Fig. 3c). The hot spot temperature can be decreased and controlled significantly by applying the PBMR, what is shown in Fig. 3c. Similar results can be found for the oxidative coupling of methane [24]. The hot spot temperature of the FBR increases drastically
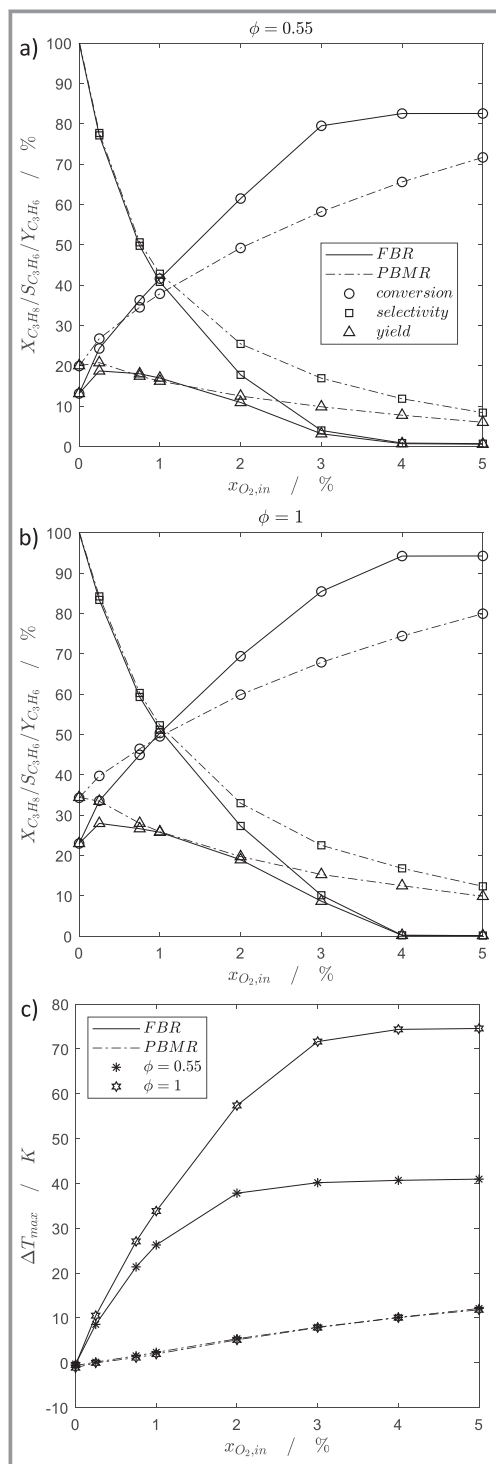
Figure 3. a) and b) Comparison between the FBR and PBMR (ts/ss = 1/8) in pilot-scale (D/d_P = 21) with various catalyst fractions (WHSV(Φ = 0.55) = 400 kg s m^{-3}, WHSV(Φ = 1) = 722 kg s m^{-3}) for different oxygen concentrations and c) hot spot temperatures of the FBR and PBMR in pilot-scale (D/d_P = 21) with various catalyst fractions for different oxygen concentrations ($x_{C3H8,in}$ = 1 %, $T_W = T_{in}$ = 600 °C), $\lambda(r)$ model.

with an increased oxygen concentration and mass of catalyst, whereas the PBMR is nearly independent of both, due to radial convection by distributed dosing, which leads to a direct cooling of the catalyst bed. Thus, no heat accumulation in a particular region is pronounced in the PBMR.
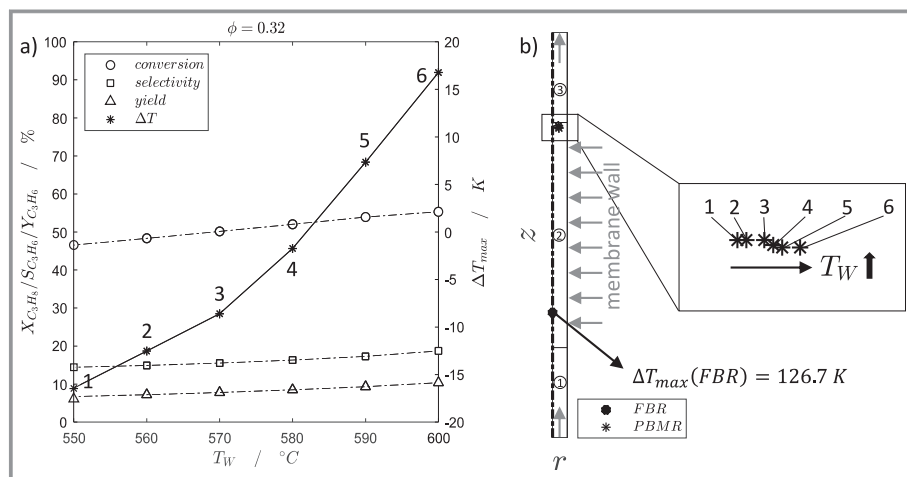
3.3 Various Wall/Membrane Flow Temperatures

Since the significantly highest hot spot temperature of the FBR occurs at D/d_P = 40 (Fig. 2), the influence of the membrane flow temperature is studied in detail for this case. In Fig. 4a the performance and hot spot temperatures of the PBMR with D/d_P = 40 for various wall and respectively membrane flow temperatures, as a new degree of freedom, are shown.

Fig. 4a illustrates, that the hot spot temperature can be decreased in a controlled manner by lowering the membrane flow temperature. This also leads to a deeper penetration of oxygen into the catalyst bed (Fig. 4b), by taking the hot spot positions into account. As described before, the hot spot in the PBMR is not localized as in the FBR. Due to the distributed dosing, oxygen is radially limited, which reduces the influence of series oxidations and shifts the hot spot convectively to the reactor outlet. With higher temperature, oxygen is faster converted, so that the hot spots occur closer to the wall (Fig. 4b). In comparison to the FBR, the hot spot temperature of the PBMR is drastically lower. Unfortunately, the reactor performance slightly decreases along a drastically lowered membrane flow temperature, mainly due to a lower reaction rate of the highly endothermic TDH. Thus, a new optimization problem results with respect to the membrane flow temperature.

4 Conclusion

The aim of this theoretical study was to investigate the influence of scale-up and axial oxygen distribution on reactor performance and hot spot formation. A conventional FBR and the PBMR were applied to the ODH and TDH of propane to propene. 2D simulations based on the more complex $\lambda(r)$ model revealed a better agreement with experimental data than those based on the simplified α_W model. As shown in this contribution, the yield of propene can be increased in pilot-scale from 18 to 21 % with a catalyst ratio of Φ = 0.55 and from 28 to 35 % with a catalyst ratio of Φ = 1, by using a PBMR instead of the FBR. Furthermore, it is found, that the hot spot temperature of the FBR increases significantly with an increased D/d_P ratio. By a distributed membrane flow, the hot spot temperature and location can be controlled and the formation of a local hot spot can be depressed.

Consequently, selectivity and temperature control via adjusting suitable membrane flows is promising. This offers new degrees of freedom for membrane distributors. Since

Figure 4. a) Comparison of the reactor performance of the PBMR (ts/ss = 1/8) with different membrane flow temperatures (T_W) and corresponding hot spot temperatures (T_{in} = 600 °C, D/d_P = 40, Φ = 0.32, WHSV = 400 kg s m^{-3}, $x_{C3H8,in}$ = 1 %, $x_{O2,in}$ = 4 %) and b) corresponding local hot spot positions in a 2D-illustration, $\lambda(r)$ model.

the temperature and concentration fields are complex, only a detailed 2D modelling provides sufficient understanding and potential for further optimization.

Supporting Information

Supporting information for this article can be found under DOI: 10.1002/cite.202000227. This section includes additional references to primary literature relevant for this research [25–32].

Acknowledgement

Symbols used

a	[–]	exponent
A	[m^2]	area
b	[–]	exponent
c	[mol m^{-3}]	concentration
c_P	[J (mol K)$^{-1}$]	specific heat capacity
d	[m]	diameter
D	[m]	tube diameter
D^{eff}	[m^{2}s^{-1}]	effective mass dispersion coefficient
J	[mol (m^{2}s)$^{-1}$]	molar flux
k	[m^{3n}Pa^{-n}]	reaction rate constant
K	[–]	performance indicator (conversion, selectivity, yield)
K_{WGS}	[–]	equilibrium constant
m	[kg]	mass
$\dot{n}$	[mol s^{-1}]	molar flow

N_{exp}	[–]	number of experiments
p	[Pa]	pressure
r	[mol (kg s)$^{-1}$]	reaction rate
r	[m]	radial coordinate
R	[m]	tube radius
S	[–]	selectivity
T	[K]	temperature
u	[m s^{-1}]	superficial velocity
$\dot{V}$	[m^{3}s^{-1}]	volumetric flow
V_R	[m^3]	reactor volume
x	[–]	molar fraction
X	[–]	conversion
Y	[–]	yield
z	[m]	axial coordinate
Z	[m]	reactor length

Greek symbols

α	[W (m^{2}K)$^{-1}$]	heat transfer coefficient
ΔH_R	[J mol^{-1}]	reaction enthalpy
ε	[–]	porosity
η	[Pa s]	dynamic viscosity
λ^{eff}	[W (m K)$^{-1}$]	effective heat dispersion coefficient
ν	[–]	stoichiometric coefficient
ρ	[kg m^{-3}]	density
ρ_{bulk}	[kg m^{-3}]	bulk density
Φ	[–]	catalyst fraction

Subscripts

c	cross section
cat	catalyst
exp	experimental
f	fluid
high	higher D/d_P ratio
i	component index
in	inlet
j	reaction index

Communication

Chemie Ingenieur Technik

low	lower D/d_P ratio
mem	membrane
p	particle
r	radial direction
s	solid
sim	simulated
ss	shell-side
ts	tube-side
w	wall
0	ambient

Abbreviations

BC	boundary condition
eq.	equation
FBR	fixed bed reactor
ODH	oxidative dehydrogenation
OF	objective function
PBMR	packed-bed membrane reactor
RSS	residual sum of squares
TDH	thermal dehydrogenation
ts/ss	tube-to-shell-side ratio
WHSV	weight hourly space velocity

Literature

[1] A. Seidel-Morgenstern, *Membrane Reactors: Distributing Reactants to Improve Selectivity and Yield*, Wiley-VCH, Weinheim **2010**.

[2] K. Hertwig, L. Martens, C. Hamel, *Chemische Verfahrenstechnik: Berechnung, Auslegung und Betrieb Chemischer Reaktoren*, 3rd ed., De Gruyter, Berlin **2018**.

[3] M. Baerns, *Technische Chemie*, 2nd ed., Wiley-VCH, Weinheim **2013**.

[4] O. Levenspiel, *Chemical Reaction Engineering*, 3rd ed., Wiley, Hoboken **1999**.

[5] U. Dingerdissen, A. Martin, D. Herein, H. J. Wernicke, in *Handbook of Heterogeneous Catalysis* (Eds: G. Ertl, H. Knzinger, F. Schth, J. Weitkamp), Wiley-VCH, Weinheim **2008**.

[6] F. J. Keil, *Rev. Chem. Eng.* **2018**, *34 (2)*, 135–200. DOI: https://doi.org/10.1515/revce-2017-0085

[7] K. Sundmacher, A. Kienle, A. Seidel-Morgenstern, *Integrated Chemical Processes: Synthesis, Operation, Analysis, and Control*, Wiley-VCH, Weinheim **2005**.

[8] D. W. Agar, W. Ruppel, *Chem. Ing. Tech.* **1988**, *60 (10)*, 731–741. DOI: https://doi.org/10.1002/cite.330601003

[9] K. R. Westerterp, *Chem. Eng. Sci.* **1992**, *47 (9–11)*, 2195–2206. DOI: https://doi.org/10.1016/0009-2509(92)87035-O

[10] D. W. Agar, *Chem. Eng. Sci.* **1999**, *54 (10)*, 1299–1305. DOI: https://doi.org/10.1016/S0009-2509(99)00040-8

[11] U. Hoffmann, K. Sundmacher, *Chem. Ing. Tech.* **1997**, *69 (5)*, 613–622. DOI: https://doi.org/10.1002/cite.330690503

[12] U. Kuerten, M. van Sint Annaland, J. A. M. Kuipers, *Int. J. Chem. React. Eng.* **2004**, *2 (1)*, A24. DOI: https://doi.org/10.2202/1542-6580.1043

[13] J. Caro, *Chinese J. Catal.* **2008**, *29 (11)*, 1169–1177. DOI: https://doi.org/10.1016/S1872-2067(09)60020-6

[14] A. Brune, T. Wolff, A. Seidel-Morgenstern, C. Hamel, *Chem. Ing. Tech.* **2019**, *91 (5)*, 645–650. DOI: https://doi.org/10.1002/cite.201800184

[15] C. Hamel, Á. Tóta, F. Klose, E. Tsotsas, A. Seidel-Morgenstern, *Chem. Eng. Res. Des.* **2008**, *86 (7)*, 753–764. DOI: https://doi.org/10.1016/j.cherd.2008.03.025

[16] Ž.S. Kotanjac, M. van Sint Annaland, J. A. M. Kuipers, *Chem. Eng. Sci.* **2010**, *65 (1)*, 441–445. DOI: https://doi.org/10.1016/j.ces.2009.04.015

[17] D. Türks, H. Mena, U. Armbruster, A. Martin, *Catalysts* **2017**, *7 (5)*, 152. DOI: https://doi.org/10.3390/catal7050152

[18] C. L. Tien, M. .L. Hunt, *Chem. Eng. Process.* **1987**, *21 (2)*, 53–63. DOI: https://doi.org/10.1016/0255-2701(87)80007-7

[19] M. Winterberg, E. Tsotsas, A. Krischke, D. Vortmeyer, *Chem. Eng. Sci.* **2000**, *55 (5)*, 967–979. DOI: https://doi.org/10.1016/S0009-2509(99)00379-6

[20] M. Winterberg, E. Tsotsas, *Int. J. Therm. Sci.* **2000**, *39 (5)*, 556–570. DOI: https://doi.org/10.1016/S1290-0729(00)00251-9

[21] D. Vortmeyer, E. Haidegger, *Chem. Eng. Sci.* **1991**, *46 (10)*, 2651–2660. DOI: https://doi.org/10.1016/0009-2509(91)80058-7

[22] M. Nilles, *Wärmeübertragung an der Wand durchströmter Schüttungsrohre*, Fortschritt-Berichte/VDI Reihe 3, Verfahrenstechnik, Nr. 264, VDI, Düsseldorf **1991**.

[23] H. Martin, M. Nilles, *Chem. Ing. Tech.* **1992**, *64 (9)*, 813. DOI: https://doi.org/10.1002/cite.330640964

[24] A. Cruellas, T. Melchiori, F. Gallucci, M. van Sint Annaland, *Energy Technol.* **2020**, *8 (8)*, 1900148. DOI: https://doi.org/10.1002/ente.201900148

[25] C. Hamel, T. Wolff, A. Seidel-Morgenstern, *Int. J. Chem. React. Eng.* **2011**, *9 (1)*, A12. DOI: https://doi.org/10.1515/1542-6580.2495

[26] H. Steen, *Handbuch des Explosionsschutzes*, Wiley-VCH, Weinheim **2000**.

[27] K. Hou, R. Hughes, *Chem. Eng. J.* **2001**, *82 (1-3)*, 311–328. DOI: https://doi.org/10.1016/S1385-8947(00)00367-3

[28] B. C. Chandrasekhara, D. Vortmeyer, *Wärme- und Stoffübertragung* **1979**, *12 (2)*, 105–111. DOI: https://doi.org/10.1007/BF01002325

[29] S. Ergun, *Chem. Eng. Prog.* **1952**, *48 (2)*, 89–94.

[30] H. C. Brinkman, *Appl. Sci. Res.* **1949**, *1 (1)*, 27. DOI: https://doi.org/10.1007/BF02120313

[31] M. Giese, *Strömung in porösen Medien unter Berücksichtigung effektiver Viskositäten*, Ph.D. Thesis, TU München **1998**.

[32] M. Winterberg, E. Tsotsas, *AIChE J.* **2000**, *46 (5)*, 1084–1088. DOI: https://doi.org/10.1002/aic.690460519